Tracking the Interaction between a CO-Functionalized Probe and Two Ag-Phthalocyanine Conformers by Local Vertical Force Spectroscopy

Karl Rothe, Nicolas Néel, Marie-Laure Bocquet, Jörg Kröger

Tracking the Interaction between a CO-Functionalized Probe and Two Ag-Phthalocyanine Conformers by Local Vertical Force Spectroscopy

Karl Rothe,[†] Nicolas Néel,[†] Marie-Laure Bocquet,[*,‡] and Jörg Kröger[*,†]

†*Institut für Physik, Technische Universität Ilmenau, D-98693 Ilmenau, Germany*

‡*Laboratoire de Physique de l'École Normale Supérieure, ENS, Université PSL, CNRS, Sorbonne Université, Université Paris-Diderot, Sorbonne Paris Cité, F-75005 Paris, France*

E-mail: marie-laure.bocquet@ens.fr; joerg.kroeger@tu-ilmenau.de

Keywords: Atomic force microscopy, Scanning tunneling microscopy, CO-terminated tip, Chemical-bond formation, Relaxation, Density functional theory

Abstract

Intentionally terminating scanning probes with a single atom or molecule belongs to a rapidly growing field in the quantum chemistry and physics at surfaces. However, the detailed understanding of the coupling between probe and adsorbate is in its infancy. Here, an atomic force microscope probe functionalized with a single CO molecule is approached with picometer control to two conformational isomers of Ag-phthalocyanine adsorbed on Ag(111). The isomer with the central Ag atom pointing to CO exhibits a complex evolution of the distance-dependent interaction, while the conformer with Ag bonded to the metal surface gives rise to a Lennard-Jones behavior. In virtue of spatially resolved force spectroscopy and the comparison with results obtained from microscope probes terminated with a single Ag atom, the mutual coupling of the protruding O atom of the tip and the Ag atom of the phthalocyanine molecule is identified as the cause for the unconventional variation of the force. Simulations of the entire junction within density functional theory unveil the presence of ample relaxations in the case of one conformer, which represents a rationale for the peculiar vertical-distance evolution of the interaction. The simulations highlight the role of physisorption, chemisorption and unexpected junction distortions at the verge of bond formation in the interpretation of the distance-dependent force between two molecules.

Introduction

Slightly more than two decades between the advent of the atomic force microscope (AFM)[1] and the imaging of adsorbed single molecules with unprecedented submolecular resolution owing to a CO-terminated AFM tip[2] reflect the stupendous development of AFM into a powerful quantum chemistry method. Undoubtedly, the invention of the qPlus sensor[3,4] – a quartz tuning fork with one fixed and one freely oscillating prong – has paved the way for many seminal findings, *e. g.*, the measurement of the force needed to move atoms on surfaces,[5] the sensing of stochastic motion of a single adsorbed H_2 molecule,[6] the discrimination of

bond order[7] and covalent bond structure[8] at the single-molecule scale as well as the probing of physisorbed and chemisorbed states in a CO–Fe bond.[9] The intentional termination of the tip with a single atom or molecule besides boosting the spatial resolution in imaging[2,10] additionally led to insights into the interaction of two CO molecules,[11] the anisotropic charge distributions at surfaces,[12] the force fields atop adsorbed molecules[13] and the resolution of H atoms at the onset of Pauli repulsion between the functionalized probe and the imaged molecule.[14] Moreover, CO-terminated AFM tips were used to explore chemically active sites at metal clusters[15] and organic molecules[16] on surfaces.

In a recent work,[9] a CO-terminated tip was approached to a single Fe atom adsorbed on Cu(111). The vertical force between the CO molecule and the adsorbed atom (adatom) exhibited two minima separated by a repulsive barrier, which was rationalized in terms of the transition between physisorption and chemisorption when decreasing the CO–Fe distance. For Si and Cu adatoms, the evolution of the vertical force resembled a Lennard-Jones behavior with only a single minimum. Extrema in the vertical force variation between a CO-terminated tip and a surface can also reflect the bending of the CO probe.[17] Similar effects were reported for Cl-terminated tips, where the Cl atom may translate at the tip apex.[18] The flexibility of CO was previously identified as the cause for the AFM contrast mechanism[10,19–21] as well as for the modification of apparent bond lengths[11,22] in the Pauli repulsion range of probe–adsorbate separations. The close proximity of the probe was likewise shown to impact the geometry of the adsorbate complex, such as the tilting of molecular adsorbates in the vicinity of a metal tip[23] or different preferred orientations of an adsorbed molecule depending on the distance to a CO-terminated probe.[24] At bonding distances, attractive forces between tip and surface become strong enough to even irreversibly distort the structural integrity of the junction and transform it into a hybrid object.[25,26] Hence, taking into account accurate relaxations of the junction geometry as modeled within density functional theory (DFT) is crucial for the interpretation of distance-dependent interactions,[23,27] in particular for junction widths in the Pauli repulsion distance range.

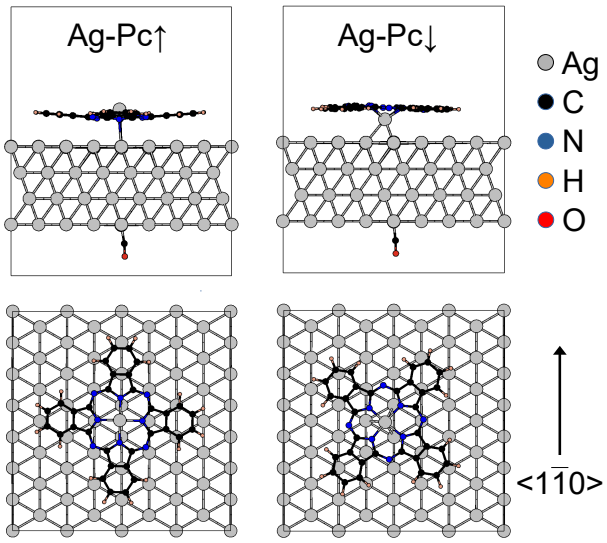

Figure 1: Supercell geometries of the junction in the tunneling range of distances. Top: Side view of relaxed junction geometries for Ag-Pc↑ (left) and Ag-Pc↓ (right) adsorbed on Ag(111) and viewed along the $\langle 010 \rangle$ direction. A selection of atoms is allowed to move in the junction. The conformational isomers exhibit an inverted (Ag-Pc↑) and normal (Ag-Pc↓) dome shape. A CO-terminated tip is modeled by a CO molecule adsorbed at a Ag(111) top site on the bottom side of the 4-layer slab. The interaction of CO with the molecular adsorbate of the adjacent supercell is quenched due to the elevated distance between O and the central Ag atom beneath, 1.14 nm for Ag-Pc↑ and 1.24 nm for Ag-Pc↓. Bottom: Top view of Ag-Pc↑ (left) with the Ag center adopting a lattice bridge site. One pair of phenyl moieties is oriented along the surface $\langle 1\bar{1}0 \rangle$ lattice direction. The Ag-Pc↓ (right) center resides at a hollow site. The orientation of an opposite phenyl pair encloses an angle of 40° with $\langle 1\bar{1}0 \rangle$. The supercell (gray lines in the top and bottom panels) spans a surface area of 1.994 nm × 2.015 nm and a height of 2.440 nm along the surface normal.

The main motivation for the combined experimental and theoretical studies presented in this work is the scrutiny of structural relaxations in a junction of two molecules and of their impact on the mutual force evolution with the molecule–molecule separation. The junction comprises an AFM tip terminated with a single CO molecule and two conformational isomers of Ag-phthalocyanine (Ag-Pc) on Ag(111) (Figure 1). Conformer Ag-Pc↑ exposes its central Ag atom to the vacuum and moderately binds the substrate via two of its pyrrolic N atoms, while in Ag-Pc↓ the Ag atom is chemically anchored to the surface. For Ag-Pc↑, the vertical force evolution with decreasing distance to single CO exhibits an unexpectedly rich structure. In contrast, the Ag-Pc↓ conformational isomer shows a Lennard-Jones-type interaction behavior. Local force spectroscopy at different intramolecular sites together with the comparison of vertical-force traces obtained with an AFM probe terminated by a single Ag atom evidence that the interaction between O of CO and Ag of Ag-Pc↑ is decisive for the unconventional force evolution. Density functional theory indeed reveals a complex bond formation process between CO and Ag-Pc↑, where strong structural junction relaxations occur, including the lifting of Ag-Pc↑ from the surface at physisorption distances and its reattachment at chemisorption separation. In contrast, the DFT-derived relaxations show that the conformational counterpart, Ag-Pc↓, virtually preserves its adsorbed geometry upon CO approach and is insensitive to bonding.

Methods

A combined AFM and scanning tunneling microscope (STM) was operated in ultrahigh vacuum (10^{-9} Pa) and at low temperature (4.8 K). Surfaces of Ag(111) were cleaned by Ar^+ ion bombardment and annealing. Chemically etched PtIr wire was used as the tip material and presumably coated with substrate material (Ag) in the course of in-situ tip preparation, which includes tip–surface contacts. The qPlus sensor [4,28] was driven at a resonance frequency 29.9 kHz with quality factor 45000 and amplitude 30 pm. The vertical force between tip and

sample was extracted from distance-dependent resonance frequency changes.[29,30] Metal-free 2H-Pc molecules (purity 98 %) were sublimated from a heated Ta crucible and deposited on clean Ag(111) at room temperature. Subsequently, CO molecules were adsorbed on the cold (6 K) 2H-Pc-covered surface by backfilling the vacuum vessel with gaseous CO (purity 99.97 %) at a partial pressure of 10^{-7} Pa with opened cryostat radiation shields. Topographic STM and AFM data were processed using WSxM.[31]

Density functional calculations were carried out using the Vienna ab-initio simulation package[32] with the Perdew-Burke-Ernzerhof (PBE) exchange-correlation.[33] The projector-augmented wave potential with a standard cutoff energy of 400 eV was used to describe the electron–ion interaction.[34] Partial occupancies were determined by Gaussian scheme considering a low smearing of 0.05 eV, which is a crucial parameter for accurate relaxations in the junction. To account for van der Waals interactions and achieve structural as well as electronic convergence the generalized-gradient-approximation PBE-D3 method[35] was used. The metallic surface was modeled by four atomic Ag layers and a rectangular $(7 \times 4\sqrt{3})$-Ag(111) unit cell embedded in about 1.4 nm of vacuum space. The used Ag lattice parameter of 0.4070 nm corresponds to a nearest-neighbor distance on Ag(111) of 0.2879 nm. The atomic positions of the topmost slab layer, the Ag-Pc molecule, the CO-terminated tip and its two nearest Ag atom neighbors of the bottom slab layer were relaxed until forces were smaller than 0.5 eV/nm at a single **k**-point (Γ) of the supercell Brillouin zone. These convergence criteria on the forces are sufficient for geometry determination. The simulation of STM images was performed by applying the Tersoff-Hamann theory in a plane-wave basis set as implemented in the STMpw code.[36] Visualization of simulated data proceeded via the Crystal Maker 10 software.[37]

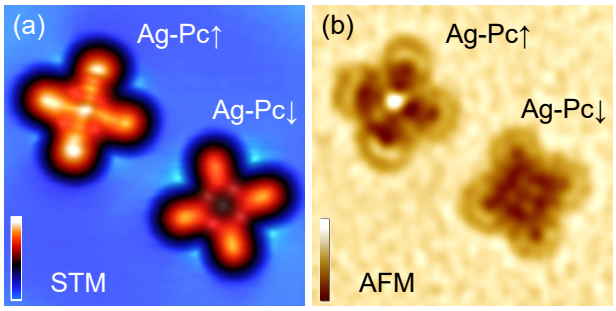

Figure 2: STM and AFM images of Ag-Pc↑ and Ag-Pc↓. (a) STM image (bias voltage: 50 mV, tunneling current: 15 pA, size: 4 nm × 4 nm, 4.8 K) of marked conformational isomers on Ag(111). The color scale encodes apparent heights from 0 pm (blue) to 115 pm (white). (b) AFM image of the same molecules as in (a) acquired in the Pauli repulsion distance range. The color scale encodes resonance frequency changes from −8 Hz (brown) to −2 Hz (white). Both images were acquired with a CO-terminated tip.

Results and Discussion

Isomers Ag-Pc↑ and Ag-Pc↓ are the stable products of an on-surface single-molecule metalation; that is, according to a previously reported procedure[38] the pyrrolic H of 2H-Pc was abstracted atom by atom through the local electron injection into the center of the benzopyrrole macrocycle. The Ag atom was subsequently transferred to the free-base Pc molecule from the AFM tip.[38] While Ag-Pc↑ results directly from this metalation, Ag-Pc↓ is obtained by applying an elevated positive bias voltage (> 3 V) across the molecular junction.[38] A similar transfer of the central metal ion through the molecular plane was reported for Sn-Pc on Ag(111).[39] The termination of the tip with a single CO molecule proceeded *via* adsorbed CO and the transfer to the tip[40] (Supporting Information, Figure S1). Figure 2 shows the appearance of the isomers in STM (Figure 2a) and AFM (Figure 2b) images obtained with a CO-terminated tip. For Ag-Pc↑ the metal center appears as a protrusion in STM and AFM data, which reflects its elevated position above the inverted-dome plane of the adsorbed molecule as revealed by DFT (Figure 1). The simulated Ag-Pc↑ conformer arises from a two-step relaxation; first, planar Pc is relaxed on the surface and N–surface bonds are formed leading to the inverted Pc dome shape; second, the Ag atom is added above the adsorbed Pc and relaxes into its slightly elevated position. In contrast, the simulated Ag-Pc↓

conformer results from a relaxation of the planar Ag-Pc moiety upon adsorption on Ag(111). For this conformer, solely the central metal atom binds to the surface while the constituent atoms of the Ag-Pc↓ ligands do not contribute to the bonding. The ↓-conformer appears with a central depression, which is consistent with the sandwiched position of the Ag atom beneath the molecular plane forming covalent bonds with the Ag(111) surface. The experiments revealed that AFM images depend strongly on the tip-molecule distance (Supporting Information, Figure S2), which is in agreement with a previous report on naphthalocyanine molecules.[41]

The main experimental finding of the present studies is the evolution of the vertical force between the CO-terminated tip and the Ag center of the two conformational isomers (Figure 3). The most striking result was obtained from Ag-Pc↑ (Figure 3a). Deviating clearly from the conventional Lennard-Jones behavior, the distance-dependent resonance frequency change $\Delta f(z)$ of the AFM oscillating tuning fork exhibits two consecutive minima with negative Δf separated by a distance region where $\Delta f > 0$. Figure 3b shows the numerically evaluated[29,30] vertical short-range force $F(z)$. Long-range and slowly varying contributions to the total vertical force were removed using a previously reported method (Supporting Information, Figure S3).[42–44] The evolution of $F(z)$ reproduces the minima of $\Delta f(z)$, *i. e.*, a shallow attractive F minimum at $-232\,\mathrm{pm}$ and a deeper attractive minimum at $215\,\mathrm{pm}$. Although the repulsive force barrier between the minima is of comparable height ($\approx 11\,\mathrm{pN}$) as previously reported for CO–Fe contacts,[9] the $F(z)$ evolution between the minima is markedly different. In particular, these minima are not solely separated by a repulsive ($F > 0$) barrier. Rather, the entire $F(z)$ evolution can be divided into three ranges α, β and γ (Figure 3b). In α, $F(z)$ decreases, passes through the shallow minimum and then increases up to range β, where $F(z)$ is nearly constant and weakly attractive; range γ starts at the first zero of $F(z)$ at z_p, exhibits a broad repulsive barrier up to the second zero at z_b, passes through the deep minimum and increases steeply intersecting again $F = 0$ at z_c. The zeros of $F(z)$ correspond to extrema positions of the associated energy $E = -\int F\,\mathrm{d}z$, which is shown in Figure 3c.

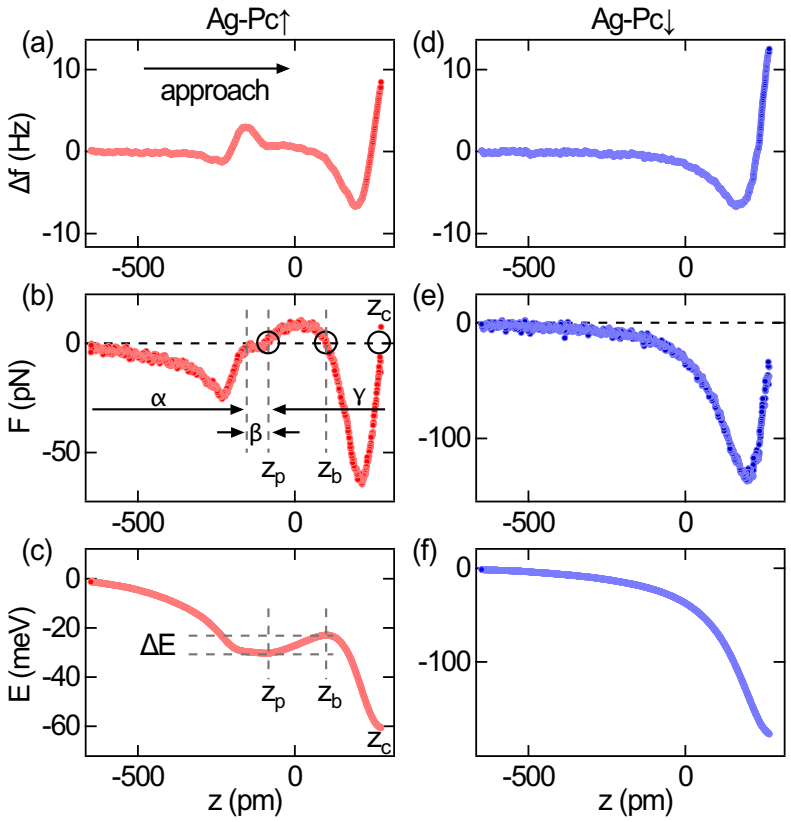

Figure 3: Vertical-distance dependence of short-range resonance frequency change, force and energy. (a) Resonance frequency change Δf, (b) vertical force F and (c) energy E as a function of the tip displacement z acquired atop the center of Ag-Pc↑. The approach direction is indicated in (a) and applies to all panels. Displacement $z = 0$ is defined by the tip position at which the STM feedback loop is deactivated (50 mV, 15 pA for all data sets). Displacements z_p, z_b and z_c denote zeros of F. Ranges α, β, γ are explained in the text. Energy $E(z)$ was obtained from a numerical integration of $F(z)$ in (b). Local E extrema at z_p, z_b and z_c correspond to zeros of F. The marked energy barrier is defined as $\Delta E = E(z_\mathrm{b}) - E(z_\mathrm{p})$. (d)–(f) Same as (a)–(c) for Ag-Pc↓.

In contrast, $\Delta f(z)$ and $F(z)$ for Ag-Pc↓ (Figure 3d,e) follow the Lennard-Jones evolution, *i. e.*, a monotonous decrease with increasing z until the point of maximum attraction is reached and followed by a steep increase due to the progressive influence of Pauli repulsion. The associated energy variation is depicted in Figure 3f. It shows a monotonous decrease approaching a minimum at elevated tip excursion.

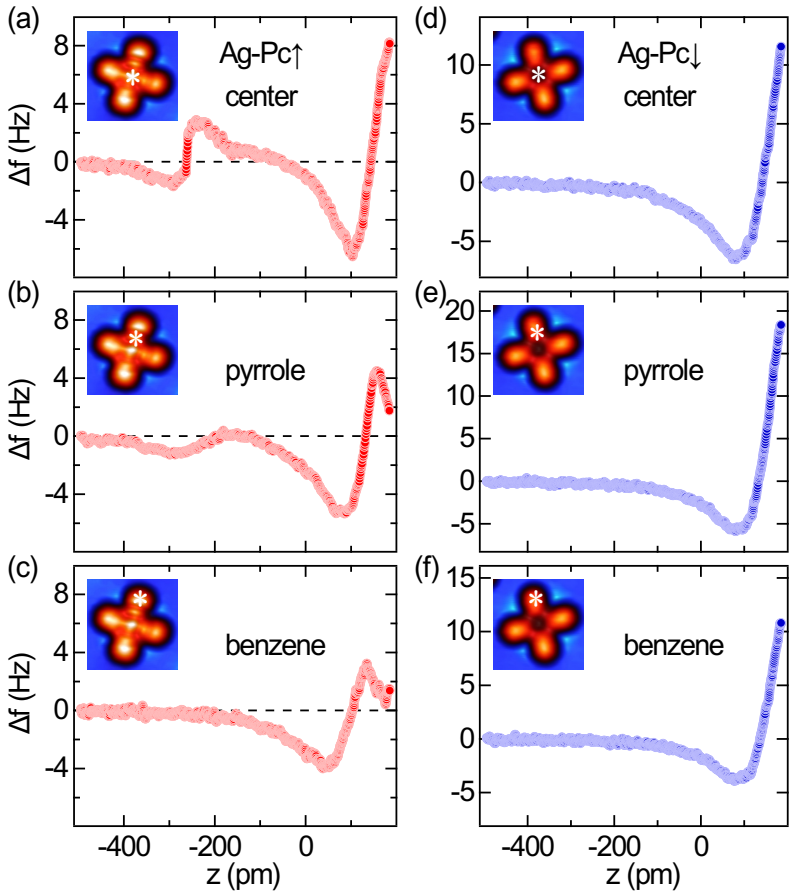

Figure 4: Spatially resolved short-range resonance frequency changes as a function of the tip excursion. (a)–(c) $\Delta f(z)$ acquired atop Ag-Pc↑ at the Ag center, the center of the pyrrole and benzene moieties. Inset: STM image of Ag-Pc↑ (50 mV, 15 pA, 2 nm × 2 nm) with indicated (asterisk) position of the $\Delta f(z)$ measurement. (d)–(f) Same as (a)–(c) for Ag-Pc↓.

The experimental data presented in Figure 3 indicate an intriguing interaction behavior between CO and Ag-Pc↑, while a more simple coupling scenario applies to the CO–Ag-Pc↓ contact. It is therefore reasonable to assume that the protruding atoms of the junction – O of the CO-terminated tip and the vaccum-exposed Ag atom of Ag-Pc↑ – drive the short-

range interaction between the two molecules. In the case of Ag-Pc↓ the central Ag atom is located below the molecular plane and electronically protected by its hybridization with the substrate surface atoms. Therefore, this lower-lying central Ag atom presumably exhibits a reduced chemical reactivity towards the molecular tip.

To further corroborate the assumption of a preferred O–Ag bond for Ag-Pc↑, spatially resolved Δf spectroscopy was performed across Ag-Pc↑ (Figure 4a–c) and Ag-Pc↓ (Figure 4d–f). The $\Delta f(z)$ traces acquired atop the center of Ag-Pc↑ (Figure 4a) shows the complex behavior as revealed in Figure 3a for another Ag-Pc↑ molecule. Parking the tip atop an intramolecular site close to the center of the Ag-Pc↑ pyrrole moiety (Figure 4b) already leads to a strong reduction of the region with $\Delta f > 0$, while the shallow minimum of $\Delta f(z)$ persists. Above the benzene center (Figure 4c) the shallow minimum has entirely disappeared. The deep minimum exhibits a gradual attenuation from $\approx -6.5\,\mathrm{Hz}$ (center) *via* $\approx -5.1\,\mathrm{Hz}$ (pyrrole) to $\approx -3.9\,\mathrm{Hz}$ (benzene), which evidences a reduction of the attraction between CO and Ag-Pc↑ upon moving the probe from the center to the periphery of the molecule. Additional structure of $\Delta f(z)$ is seen for tip excursions deep in the Pauli repulsion range, which is assigned to the bending of the CO probe.[11,17] For Ag-Pc↓, in contrast, the simple Lennard-Jones-type evolution of the interaction remains, albeit with a similar reduction of the maximum attraction from $\approx -6.5\,\mathrm{Hz}$ (center) *via* $\approx -5.9\,\mathrm{Hz}$ (pyrrole) to $\approx -3.9\,\mathrm{Hz}$ (benzene).

The experiments with a CO-terminated tip were complemented by experiments with clean metal tips in order to additionally corroborate the importance of the O–Ag interaction for the $F(z)$ variation in case of Ag-Pc↑. Metal tips were prepared by repeated indentation into the Ag(111) substrate, which likely led to a coating of the PtIr tip apex with Ag. Such tips were further trained by the controlled single-atom transfer from the tip to the surface giving rise to an apex terminated by a single Ag atom.[26,45–48] Figure 5 presents typical Δf traces obtained for approaching the Ag-terminated tip to the centers of Ag-Pc↑ (Figure 5a) and Ag-Pc↓ (Figure 5b). The most obvious change compared to the experiments with CO-

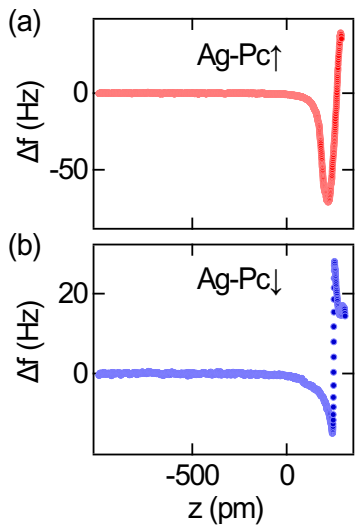

Figure 5: Vertical short-range resonance frequency change acquired with a Ag-terminated tip. (a) $\Delta f(z)$ acquired atop the center of Ag-Pc↑. Displacement $z = 0$ is defined by the tip position at which the STM feedback loop was deactivated (50 mV, 15 pA). (b) Same as (a) for Ag-Pc↓.

terminated tips is the absence of consecutive Δf minima for Ag-Pc↑. The approach of the Ag probe to Ag-Pc↓ leads to a similar Δf variation as observed with a CO-terminated tip, albeit with an abrupt increase of the $\Delta f(z)$ trace at elevated tip excursion, which signals the Ag atom transfer from the tip to the molecule.

Before concluding the experimental part, a remark on the reproducibility of the contact experiments is noteworthy. Once a CO-terminated tip was prepared, the evolution of Δf could be repeated for different adsorbed molecules demonstrating the stability of the junction and the 100 % reproducibility of the experiments. Only in cases where the tip was approached too closely to the molecule, irreversible changes of the tip structural integrity prevented the repetition of the preceding $\Delta f(z)$ trace. In some experiments, $\Delta f(z)$ was recorded during an approach and the subsequent retraction of the tip. The Supporting Information (Figure S4) show that both data sets virtually coincide, which further confirms the reproducibility and reversibility of these measurements.

The experimental findings reveal that an explanation of the peculiar $F(z)$ variation observed for Ag-Pc↑ with a CO-terminated tip solely on the basis of physisorption and

chemisorption does not hold and, therefore, stimulate to go beyond the previously reported picture.[9] In order to elucidate the atomic-scale processes underlying the experimental data, extensive atomistic simulations of the entire AFM junction including the CO-terminated tip were performed with DFT. Simulated STM images (Supporting Information, Figure S5) of both conformers at tunneling, that is, noncontact distances, are in agreement with experimental data, which supports the suitability of the chosen models for the adsorbed molecules. A large set of supercells with decreasing heights was constructed and relaxed for Ag-Pc↑ and Ag-Pc↓ with the key results summarized in Figure 6 and Figure 7, respectively. These results were obtained in a quasistatic approach in which each relaxed system constitutes the initial guess of the next one at increasing tip displacement D. The entire set of supercells can be found in the Supporting Information (Figure S6, Figure S7). The simulated tip excursion is referred to the maximum height of the supercell (2.440 nm), where $D = 0$. Using the distance-resolved simulations, the complex interaction behavior observed experimentally for Ag-Pc↑ (Figure 3a–c) and the rather simple variation of $F(z)$ for Ag-Pc↓ (Figure 3d–f) can be explained in a qualitative manner, as discussed next.

Figure 8 summarizes the calculated distances d in order to clearly observe trends as a function of the simulated tip displacement D. All distances denote the separations between the centers of closest atoms and are summarized in Table S1 and Table S2 of the Supporting Information. Starting from $D = 700$ pm, the Ag-Pc↑ molecule (Figure 8a) is gradually detached from the surface, which is seen from the rather rapid increase of the separation between the surface (Ag_s) and the Ag atom at the macrocycle center (Ag_m), $d(Ag_m - Ag_s)$ (368 pm at $D = 700$ pm to 389 pm at $D = 740$ pm), followed by a weaker increase to 393 pm at $D = 790$ pm. This D range is compatible with regions α and β in the experiments (Figure 3b) because the detachment of Ag-Pc↑ requires an attractive interaction with the CO probe. Moreover, the shallow F minimum in α most likely occurs for $D \leq 740$ pm where $d(Ag_m - Ag_s)$ increases strongly, which requires an elevated attraction. Region β with weak attraction $F(z) \approx \text{const} < 0$ is compatible with the small variation of $d(Ag_m - Ag_s)$ for

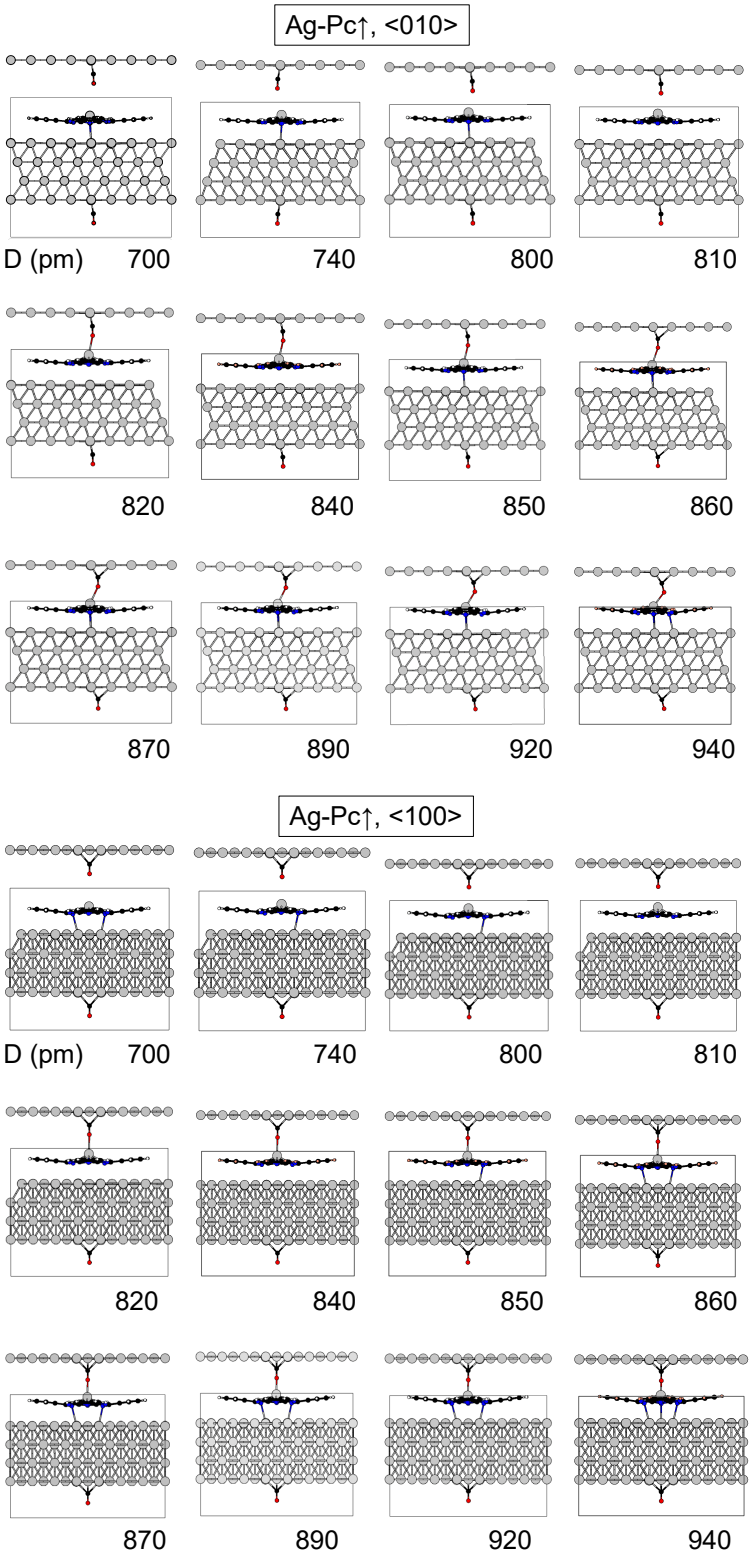

Figure 6: Selected sequence of supercells describing simulated relaxed junction geometries of CO approaching Ag-Pc↑ with indicated tip displacement D. The views are oriented along a ⟨010⟩ (top) and ⟨100⟩ (bottom) crystal direction. The disappearance and appearance of marked bonds is a direct visualization of bond elongation and shortening, respectively.[37]

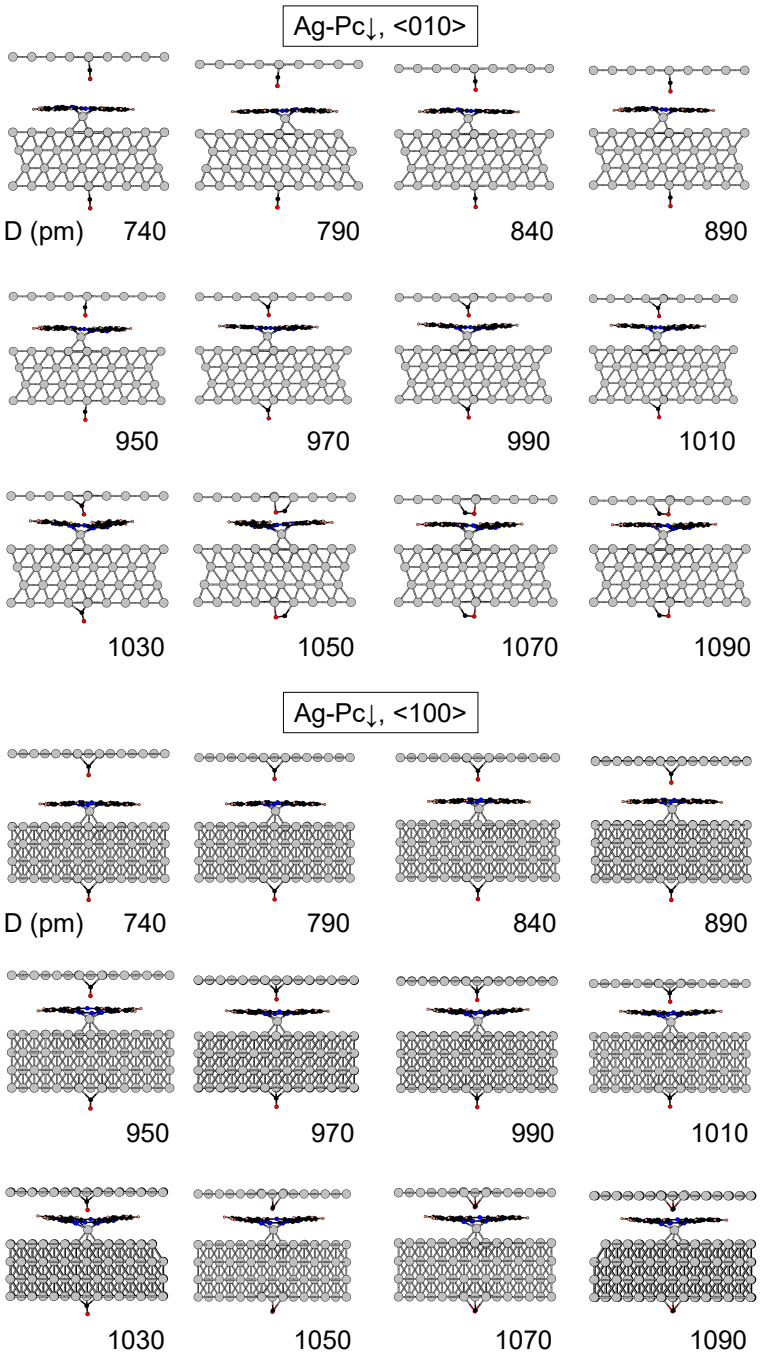

Figure 7: Same as Figure 6 for Ag-Pc↓.

$740\,\mathrm{pm} \leq D \leq 790\,\mathrm{pm}$.

For a displacement $790\,\mathrm{pm} < D_\mathrm{p} < 810\,\mathrm{pm}$ the trend of increasing $d(\mathrm{Ag_m} - \mathrm{Ag_s})$ is reversed; that is, the Ag-Pc↑ molecule is gently approached to the surface again. This trend reversal at D_p is assigned to the formation of a physical bond and may therefore be identified with z_p in the experiments. For $D > D_\mathrm{p}$, the decrease of the distance between the O atom of CO and $\mathrm{Ag_m}$, $d(\mathrm{O} - \mathrm{Ag_m})$, is weakened; it even increases for $840\,\mathrm{pm} < D \leq 870\,\mathrm{pm}$. The latter is due to a lateral translation of CO at the tip (Figure 6). For this translation to occur, it is reasonable to assume a repulsive interaction between CO and Ag-Pc↑, which is present in the experiments for $z_\mathrm{p} < z < z_\mathrm{b}$ where $F(z) > 0$. The associated energy barrier is $\Delta E = E(z_\mathrm{b}) - E(z_\mathrm{p}) \approx 7\,\mathrm{meV}$ (Figure 3c). While ΔE is nearly an order of magnitude lower than reported activations energy barriers for CO diffusion on surfaces, *e. g.*, for Cu(111),[5,49] it is similar to the frustrated-translation energy of CO on Cu(111) in proximity of the tip.[50]

Further increase of D gives rise to an abrupt decrease of $d(\mathrm{O} - \mathrm{Ag_s})$ to 233 pm at $D = 880\,\mathrm{pm}$, which may be rationalized as the response to another strong attraction – the second minimum in $F(z)$. Chemical-bond formation is likely to occur for $880\,\mathrm{pm} < D_\mathrm{c} < 920\,\mathrm{pm}$, where the trend of strongly decreasing $d(\mathrm{Ag_m} - \mathrm{Ag_s})$ turns into an essentially constant behavior. Distances $d(\mathrm{O} - \mathrm{Ag_m})$ slightly vary between 230 pm and 233 pm, which are indicative of a chemical bond.

For $D > 920\,\mathrm{m}$, distance $d(\mathrm{Ag_m} - \mathrm{Ag_s})$ is reduced and reflects the gradual insertion of the Ag central atom into the molecular plane. Below $d(\mathrm{Ag_m} - \mathrm{Ag_s}) = 373\,\mathrm{pm}$, a constrained chemical bond starts to form, which is correlated with a bending of CO at the tip (Supporting Information, Figure S8). In the experiments, this range of tip excursions was found to be detrimental to the structural integrity of the junction.

It is difficult to identify physisorbed and chemisorbed states from calculations of the relaxed junction geometry alone. Therefore, the electronic density of states (DOS) was additionally computed and projected onto the O p_z-orbital (Supporting Information, Figure S9). The results support the idea that the transition from physisorption to chemisorption

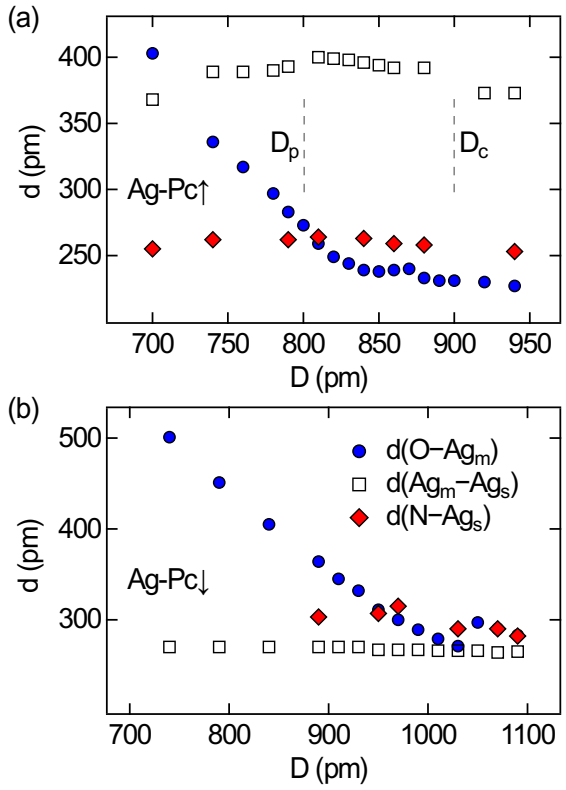

Figure 8: Calculated interatomic distances as a function of tip displacement. (a) Evolution of the distance between the O atom of CO and the Ag atom of Ag-Pc↑ (Ag_m, dots), Ag_m and the closest Ag surface atom (Ag_s, squares) as well as between the pyrrolic N atom and Ag_s (lozenges). Tip excursions D_p and D_c mark approximate positions where a physical and chemical bond, respectively, is formed. (b) Same as (a) for Ag-Pc↓.

occurs in the region 800 pm $< D <$ 900 pm.

Interestingly, for Ag-Pc↓ (Figure 7, Figure 8b), the simulations do not reveal a similarly complex bonding behavior as for Ag-Pc↑. In particular, partial detachment of Ag-Pc↓ in the course of CO approach is not taking place, which is most likely due to the strong bond of the Ag center with the Ag(111) surface. The latter is reflected by the weak variation of $d(\mathrm{Ag_m} - \mathrm{Ag_s})$ (Figure 8b). Presumably, the Ag center is sterically protected by the Pc above and, thus, electronically passivated like in sandwiched metal complexes. It is hence nonreactive to further bonding. Indeed, for $D <$ 950 pm Ag-Pc↓ retains its dome shape and the central Ag atom is lifted by only 1 pm from the Ag(111) surface. In the experiments, this range of distances therefore matches tip displacements where $F(z)$ decreases, passes through the point of maximum attraction and increases again. For further tip approach in the simulations the dome shape of Ag-Pc↓ subtly transitions into an inverted dome shape (at $D =$ 1030 pm in Figure 7). Increasing D then pushes the central Ag atom towards the surface and entails a strong bending of the flexible CO, which for even larger D binds with its O atom back to the tip substrate. This bonding scenario at elevated tip displacement is not reached in the AFM experiments due to irreversible modifications of the junction geometry.

Before concluding, a few remarks on the comparison between experiment and theory are appropriate. Despite the simplicity of the atomic models, the main ingredient at play at the onset of short-range interactions between CO and the molecular conformers is revealed. Hence, the simulations can qualitatively explain the difference of the conformational isomers in the force spectroscopy experiments as exposed above. Quantitatively, however, deviations of calculated distances from experimentally observed ones occur. The separation between physical and chemical bonds between CO and Ag-Pc↑ differs; it is z_c–$z_\mathrm{p} =$ 365 pm in the experiments and amounts to an approximate separation of 110 pm (Figure 8a) in the calculations. While short-range chemisorption distances are quite accurate and stable with respect to a variety of functionals used in the calculations, long-range noncovalent interaction is known to strongly depend on the empirical or self-consistent dispersion treatment in

the functionals. As exemplified for the water interaction on hexagonal boron nitride[51] all functionals related to the van der Waals interaction overestimate the binding as compared to the most accurate approach. The physical bond in case of Ag-Pc↑ may thus possibly be overestimated explaining the offset between experimental and theoretical distances. But more importantly, the simulations consider a simplistic tip structure, that is, a single CO adsorbed on a planar tip substrate, which contributes to the quantitative deviations, too. The second remark concerns the findings obtained with bare Ag tips, which lead to a conventional Lennard-Jones behavior upon contact to both isomers (Figure 5). These observations indicate the absence of spontaneous attraction between the Ag atom at the tip apex and in the macrocycle center. To rationalize this result an orbital argument is proposed, *i. e.*, the diffuse 5*s*-orbital of the metallic Ag tip atom prevents a chemical bond to the localized Ag 4*d*-orbitals of the molecular cation; the latter prefer a bond to the likewise localized O 2*p*-orbitals.

Conclusions

Combining analyses of AFM experiments with DFT calculations of relaxed junction geometries that access the interaction between two molecules at bonding distances with picometer precision represents a powerful method to elucidate the interaction of a functionalized molecular AFM tip and adsorbed molecules. Moreover, the onset of bonding can be tracked at the single-molecule level. Structural relaxations of the single-molecule AFM junctions unveiled by DFT simulations play a decisive role in interpreting the complex variation of the distance-dependent force between the reaction partners. For the comparative case of two metallo-phthalocyanine conformers presented here, one can conclude that the bonding to CO occurs when the metallic molecular center retains a residual electronic reactivity and is structurally labile to move towards the CO tip. In contrast, a fully coordinated metal center encapsulated between the organic ligands and the substrate is chemically inert. The

presented approach contributes to the interpretation of spatially resolved vertical force spectroscopy and, more generally, is capable of scrutinizing spatially resolved chemical reactivity at the single-molecule level.

Author information

Corresponding authors

*E-mail: marie-laure.bocquet@ens.fr

*E-mail: joerg.kroeger@tu-ilmenau.de

Notes

The authors declare no competing financial interest.

Acknowledgment

Funding by the Deutsche Forschungsgemeinschaft through KR 2912/17-1 is acknowledged. The computational work was performed using the HPC ressources from GENCI-TGCC (Grant No. 2021 A9-A0070807364).

Associated content

Supporting information

The Supporting Information are available free of charge on the ACS Publications website at DOI: [hyperlink DOI]

Tip termination with a single CO molecule; Distance dependence of atomic force microscope images; Extraction of short-range forces; Simulation of scanning tunneling microscopy images; Relaxed junction geometries; Contact geometry for large tip excursion; Projected density of states

References

1. Binnig, G.; Quate, C. F.; Gerber, C. Atomic Force Microscope. *Phys. Rev. Lett.* **1986**, *56*, 930–933.

2. Gross, L.; Mohn, F.; Moll, N.; Liljeroth, P.; Meyer, G. The Chemical Structure of a Molecule Resolved by Atomic Force Microscopy. *Science* **2009**, *325*, 1110–1114.

3. Giessibl, F. J. Atomic resolution on Si(111)-(7×7) by noncontact atomic force microscopy with a force sensor based on a quartz tuning fork. *Applied Physics Letters* **2000**, *76*, 1470–1472.

4. Giessibl, F. J. The qPlus Sensor, a Powerful Core for the Atomic Force Microscope. *Review of Scientific Instruments* **2019**, *90*, 011101.

5. Ternes, M.; Lutz, C. P.; Hirjibehedin, C. F.; Giessibl, F. J.; Heinrich, A. J. The Force Needed to Move an Atom on a Surface. *Science* **2008**, *319*, 1066–1069.

6. Lotze, C.; Corso, M.; Franke, K. J.; von Oppen, F.; Pascual, J. I. Driving a Macroscopic Oscillator with the Stochastic Motion of a Hydrogen Molecule. *Science* **2012**, *338*, 779–782.

7. Gross, L.; Mohn, F.; Moll, N.; Schuler, B.; Criado, A.; Guitián, E.; Peña, D.; Gourdon, A.; Meyer, G. Bond-Order Discrimination by Atomic Force Microscopy. *Science* **2012**, *337*, 1326–1329.

8. de Oteyza, D. G.; Gorman, P.; Chen, Y.-C.; Wickenburg, S.; Riss, A.; Mowbray, D. J.; Etkin, G.; Pedramrazi, Z.; Tsai, H.-Z.; Rubio, A.; Crommie, M. F.; Fischer, F. R. Direct Imaging of Covalent Bond Structure in Single-Molecule Chemical Reactions. *Science* **2013**, *340*, 1434–1437.

9. Huber, F.; Berwanger, J.; Polesya, S.; Mankovsky, S.; Ebert, H.; Giessibl, F. J. Chemical

Bond Formation Showing a Transition from Physisorption to Chemisorption. *Science* **2019**, *366*, 235–238.

10. Mönig, H.; Hermoso, D. R.; Díaz Arado, O.; Todorović, M.; Timmer, A.; Schüer, S.; Langewisch, G.; Pérez, R.; Fuchs, H. Submolecular Imaging by Noncontact Atomic Force Microscopy with an Oxygen Atom Rigidly Connected to a Metallic Probe. *ACS Nano* **2016**, *10*, 1201–1209.

11. Sun, Z.; Boneschanscher, M. P.; Swart, I.; Vanmaekelbergh, D.; Liljeroth, P. Quantitative Atomic Force Microscopy with Carbon Monoxide Terminated Tips. *Phys. Rev. Lett.* **2011**, *106*, 046104.

12. Mallada, B.; Gallardo, A.; Lamanec, M.; de la Torre, B.; Špirko, V.; Hobza, P.; Jelinek, P. Real-Space Imaging of Anisotropic Charge of σ-Hole by Means of Kelvin Probe Force Microscopy. *Science* **2021**, *374*, 863–867.

13. Sweetman, A. M.; Jarvis, S. P.; Sang, H.; Lekkas, I.; Rahe, P.; Wang, Y.; Wang, J.; Champness, N.; Kantorovich, L.; Moriarty, P. Mapping the Force Field of a Hydrogen-Bonded Assembly. *Nature Communications* **2014**, *5*, 3931.

14. Kawai, S.; Nishiuchi, T.; Kodama, T.; Spijker, P.; Pawlak, R.; Meier, T.; Tracey, J.; Kubo, T.; Meyer, E.; Foster, A. S. Direct Quantitative Measurement of the C=O$\cdots$H–C Bond by Atomic Force Microscopy. *Science Advances* **2017**, *3*, e1603258.

15. Berwanger, J.; Polesya, S.; Mankovsky, S.; Ebert, H.; Giessibl, F. J. Atomically Resolved Chemical Reactivity of Small Fe Clusters. *Phys. Rev. Lett.* **2020**, *124*, 096001.

16. Rothe, K.; Néel, N.; Bocquet, M.-L.; Kröger, J. Extraction of Chemical Reactivity and Structural Relaxations of an Organic Dye from the Short-Range Interaction with a Molecular Probe. *The Journal of Physical Chemistry Letters* **2022**, *13*, 8660–8665.

17. Néel, N.; Kröger, J. Atomic Force Extrema Induced by the Bending of a CO-Functionalized Probe. *Nano Letters* **2021**, *21*, 2318–2323.

18. Scheil, K.; Gruber, M.; Ondrácek, M.; Berndt, R. Force Spectroscopy of Iron Tetraphenylporphyrin Molecules with Cl Tips. *The Journal of Physical Chemistry C* **2020**, *124*, 26889–26896.

19. Hapala, P.; Kichin, G.; Wagner, C.; Tautz, F. S.; Temirov, R.; Jelínek, P. Mechanism of high-resolution STM/AFM imaging with functionalized tips. *Phys. Rev. B* **2014**, *90*, 085421.

20. Hämäläinen, S. K.; van der Heijden, N.; van der Lit, J.; den Hartog, S.; Liljeroth, P.; Swart, I. Intermolecular Contrast in Atomic Force Microscopy Images without Intermolecular Bonds. *Phys. Rev. Lett.* **2014**, *113*, 186102.

21. Lee, A. J.; Sakai, Y.; Kim, M.; Chelikowsky, J. R. Repulsive tip tilting as the dominant mechanism for hydrogen bond-like features in atomic force microscopy imaging. *Applied Physics Letters* **2016**, *108*, 193102.

22. Welker, J.; Giessibl, F. J. Revealing the Angular Symmetry of Chemical Bonds by Atomic Force Microscopy. *Science* **2012**, *336*, 444–449.

23. Hauptmann, N.; Groß, L.; Buchmann, K.; Scheil, K.; Schütt, C.; Otte, F. L.; Herges, R.; Herrmann, C.; Berndt, R. High-Conductance Surface-Anchoring of a Mechanically Flexible Platform-Based Porphyrin Complex. *New Journal of Physics* **2015**, *17*, 013012.

24. Weymouth, A. J.; Riegel, E.; Simmet, B.; Gretz, O.; Giessibl, F. J. Lateral Force Microscopy Reveals the Energy Barrier of a Molecular Switch. *ACS Nano* **2021**, *15*, 3264–3271.

25. Hofer, W. A.; Fisher, A. J.; Wolkow, R. A.; Grütter, P. Surface Relaxations, Current En-

hancements, and Absolute Distances in High Resolution Scanning Tunneling Microscopy. *Phys. Rev. Lett.* **2001**, *87*, 236104.

26. Limot, L.; Kröger, J.; Berndt, R.; Garcia-Lekue, A.; Hofer, W. A. Atom Transfer and Single-Adatom Contacts. *Phys. Rev. Lett.* **2005**, *94*, 126102.

27. Sugimoto, Y.; Pou, P.; Custance, Ó.; Jelinek, P.; Morita, S.; Pérez, R.; Abe, M. Real topography, atomic relaxations, and short-range chemical interactions in atomic force microscopy: The case of the α-Sn/Si(111)-$\sqrt{3} \times \sqrt{3}R30^\circ$ surface. *Phys. Rev. B* **2006**, *73*, 205329.

28. Giessibl, F. J. High-Speed Force Sensor for Force Microscopy and Profilometry Utilizing a Quartz Tuning Fork. *Applied Physics Letters* **1998**, *73*, 3956–3958.

29. Giessibl, F. J. A Direct Method to Calculate Tip–Sample Forces from Frequency Shifts in Frequency-Modulation Atomic Force Microscopy. *Appl. Phys. Lett.* **2001**, *78*, 123–125.

30. Sader, J. E.; Jarvis, S. P. Accurate Formulas for Interaction Force and Energy in Frequency Modulation Force Spectroscopy. *Appl. Phys. Lett.* **2004**, *84*, 1801–1803.

31. Horcas, I.; Fernández, R.; Gómez-Rodríguez, J. M.; Colchero, J.; Gómez-Herrero, J.; Baro, A. M. WSXM: A Software for Scanning Probe Microscopy and a Tool for Nanotechnology. *Rev. Sci. Instrum.* **2007**, *78*, 013705.

32. Blöchl, P. E. Projector Augmented-Wave Method. *Phys. Rev. B* **1994**, *50*, 17953–17979.

33. Perdew, J. P.; Burke, K.; Ernzerhof, M. Generalized Gradient Approximation Made Simple. *Phys. Rev. Lett.* **1996**, *77*, 3865–3868.

34. Kresse, G.; Furthmüller, J. Efficient Iterative Schemes for Ab Initio Total-Energy Calculations Using a Plane-Wave Basis Set. *Phys. Rev. B* **1996**, *54*, 11169–11186.

35. Grimme, S.; Antony, J.; Ehrlich, S.; Krieg, H. A Consistent and Accurate Ab Initio Parametrization of Density Functional Dispersion Correction (DFT-D) for the 94 Elements H-Pu. *J. Chem. Phys.* **2010**, *132*, 154104.

36. Lorente, N.; Robles, R. *STMpw*; Zenodo, 2019.

37. CrystalMaker Software Ltd, version 10.7; Software for Advanced Chemical and Materials Structures Modelling; Centre for Innovation and Enterprise, Oxford University Begbroke Science Park, Woodstock Road, Begbroke, Oxfordshire, OX5 1PF, UK; www.crystalmaker.com.

38. Sperl, A.; Kröger, J.; Berndt, R. Controlled Metalation of a Single Adsorbed Phthalocyanine. *Angewandte Chemie International Edition* **2011**, *50*, 5294–5297.

39. Wang, Y.; Kröger, J.; Berndt, R.; Hofer, W. A. Pushing and Pulling a Sn Ion through an Adsorbed Phthalocyanine Molecule. *Journal of the American Chemical Society* **2009**, *131*, 3639–3643.

40. Bartels, L.; Meyer, G.; Rieder, K.-H. Controlled Vertical Manipulation of Single CO Molecules with the Scanning Tunneling Microscope: A Route to Chemical Contrast. *Applied Physics Letters* **1997**, *71*, 213–215.

41. Mohn, F.; Gross, L.; Moll, N.; Meyer, G. Imaging the charge distribution within a single molecule. *Nature Nanotechnology* **2012**, *7*, 227 – 231.

42. Ternes, M.; González, C.; Lutz, C. P.; Hapala, P.; Giessibl, F. J.; Jelínek, P.; Heinrich, A. J. Interplay of Conductance, Force, and Structural Change in Metallic Point Contacts. *Phys. Rev. Lett.* **2011**, *106*, 016802.

43. Ladenthin, J. N.; Frederiksen, T.; Persson, M.; Sharp, J. C.; Gawinkowski, S.; Waluk, J.; Kumagai, T. Force-Induced Tautomerization in a Single Molecule. *Nat. Chem.* **2016**, *8*, 935 – 940.

44. Liebig, A.; Giessibl, F. J. In-Situ Characterization of O-Terminated Cu Tips for High-Resolution Atomic Force Microscopy. *Appl. Phys. Lett.* **2019**, *114*, 143103.

45. Kröger, J.; Jensen, H.; Berndt, R. Conductance of Tip–Surface and Tip–Atom Junctions on Au(111) Explored by a Scanning Tunnelling Microscope. *New J. Phys.* **2007**, *9*, 153.

46. Kröger, J.; Néel, N.; Sperl, A.; Wang, Y. F.; Berndt, R. Single-Atom Contacts with a Scanning Tunnelling Microscope. *New J. Phys.* **2009**, *11*, 125006.

47. Kröger, J.; Néel, N.; Limot, L. Contact to Single Atoms and Molecules with the Tip of a Scanning Tunnelling Microscope. *J. Phys.: Condens. Matter* **2008**, *20*, 223001.

48. Berndt, R.; Kröger, J.; Néel, N.; Schull, G. Controlled Single Atom and Single Molecule Contacts. *Phys. Chem. Chem. Phys.* **2010**, *12*, 1022–1032.

49. Wong, K. L.; Rao, B. V.; Pawin, G.; Ulin-Avila, E.; Bartels, L. Coverage and nearest-neighbor dependence of adsorbate diffusion. *The Journal of Chemical Physics* **2005**, *123*, 201102.

50. Okabayashi, N.; Peronio, A.; Paulsson, M.; Arai, T.; Giessibl, F. J. Vibrations of a molecule in an external force field. *Proceedings of the National Academy of Sciences* **2018**, *115*, 4571–4576.

51. Al-Hamdani, Y. S.; Ma, M.; Alfè, D.; von Lilienfeld, O. A.; Michaelides, A. Communication: Water on hexagonal boron nitride from diffusion Monte Carlo. *The Journal of Chemical Physics* **2015**, *142*, 181101.

TOC Graphic